Fast gyrofluid reconnection in high temperature plasmas

2012 J. Phys.: Conf. Ser. 401 012005

(http://iopscience.iop.org/1742-6596/401/1/012005)

Journal of Physics: Conference Series **401** (2012) 012005 doi:10.1088/1742-6596/401/1/012005

Fast gyrofluid reconnection in high temperature plasmas

L Comisso[1], F L Waelbroeck[2] and D Grasso[1]

[1] Dipartimento di Energia, Politecnico di Torino, Corso Duca degli Abruzzi 24, 10129, Torino, and Istituto dei Sistemi Complessi - CNR, Via dei Taurini 19, 00185, Roma, Italy
[2] Institute for Fusion Studies, The University of Texas at Austin, Austin, TX 78712-1060, USA

E-mail: luca.comisso@polito.it

Abstract. The nonlinear evolution of collisionless magnetic reconnection in the presence of a strong guide field is analyzed on the basis of a gyrofluid model for compressible plasmas. It is found that, in a certain regime of plasma parameters, ion gyration contributes to generate two distinctive nonlinear acceleration phases of the growth rate. Furthermore, in the advanced nonlinear phase, finite values of the ion Larmor radius are identified to be responsible for a splitting of the narrow layer structures of ion guiding-center parallel velocity and density perturbations around the magnetic equilibrium null line.

1. Introduction

Magnetic reconnection is a process that changes the topology of the magnetic field lines and results in the conversion of magnetic energy into kinetic energy, thermal energy, and particle acceleration. It is observed to occur both in laboratory and in space plasmas, where it plays a key role in a number of events, classical examples of which are sawtooth relaxations in fusion devices, substorms in the Earth's magnetosphere, and solar and stellar flares [1, 2]. A general feature of these phenomena are the short time scales involved, which are much shorter than those associated with classical collisional dissipation processes. In the absence of collisions, the finite mass of electrons limit their response to a magnetic-field-aligned electric field and allows magnetic field lines to reconnect. Another common characteristic of these events is that the reconnection rate is not only fast, but also exhibits a sudden increase in its time derivative (see, e.g., [3, 4]). Explanation of the observed growth rates constitutes one of the main challenges of magnetic reconnection theory (see, e.g., [5]).

In this work we consider the regime of high temperature plasmas in the presence of a strong guide field, that is relevant for tokamaks as well as the solar corona. In this regime the sonic and ion Larmor radius, ρ_s and ρ_i, exceed the width of the electron diffusion region [6]. Therefore, sonic and ion finite Larmor radius effects cannot be neglected and indeed are known to produce a speed up of the reconnection rate [7 - 14]. Here we report new results of gyrofluid simulations that enable us to examine the effects of ion gyration on the growth rate and the field structures of spontaneous collisionless magnetic reconnection. This paper is organized as follows. In Section 2 we present the model equations that include the nonlocal response of the plasma resulting from ion gyration. In Section 3 these equations are used to simulate spontaneous magnetic reconnection in a current sheet. Finally, conclusions are drawn in Section 4.

2. The electromagnetic gyrofluid model

We consider a Hamiltonian gyrofluid model [15] obtained by taking the two lowest velocity space moments of the five-dimensional gyrokinetic equations for electrons and ions [16], assuming constant temperatures and neglecting collisions and the electron gyroradius. Electron inertia terms, on the other hand, are retained in order to break the frozen-in condition and allow for magnetic reconnection phenomena. The system of equations is completed using Ampère's law and the quasi-neutrality condition. As in Ref. [17], the magnetic curvature effects are neglected and the dynamics is assumed two-dimensional, with an ignorable coordinate along the strong, out-of-plane, magnetic field $B_0\hat{\mathbf{z}}$ (the guide field, that is taken to be constant). Furthermore, a plasma with single ion species and charge number $Z = 1$ is assumed.

We adopt a normalization scheme such that all the lengths are normalized to a characteristic magnetic equilibrium scale length L, and all times to the Alfvén time $\tau_A = L/v_A$, where $v_A = B_0/(\mu_0 n_0 m_i)^{1/2}$, with n_0 a constant background density, μ_0 the permeability of free space, and m_i the ion mass. Thus, dependent variables are normalized in the following way:

$$\left(\hat{n}_{i,e}, \hat{u}_{i,e}, \hat{\psi}, \hat{\phi}\right) = \left(\frac{L}{d_i}\frac{n_{i,e}}{n_0}, \frac{L}{d_i}\frac{u_{i,e}}{v_A}, \frac{\psi}{B_0 L}, \frac{\phi}{B_0 L v_A}\right), \tag{1}$$

where dimensionless quantities appear on the left hand side. Hereafter the carets denoting normalized quantities will be omitted for simplicity of notation. The fields n_i and $u_i = \hat{\mathbf{z}} \cdot \bar{\mathbf{v}}_i$ represent the perturbed density and the parallel (out-of-plane) velocity of the ion *guiding centers*, whereas n_e and $u_e = \hat{\mathbf{z}} \cdot \mathbf{v}_e$ are the perturbed density and the parallel velocity of the electrons. We indicate with ψ the magnetic flux function, related to the in-plane magnetic field by $\mathbf{B}_\perp = \nabla\psi \times \hat{\mathbf{z}}$, and with ϕ the electrostatic potential.

In a right-handed Cartesian coordinate system (x, y, z), the evolution equations of the model are:

$$\frac{\partial n_i}{\partial t} + [\Phi, n_i] + [u_i, \Psi] = 0, \tag{2}$$

$$\frac{\partial}{\partial t}\left(\Psi + d_i^2 u_i\right) + [\Phi, \Psi + d_i^2 u_i] + \rho_i^2 [n_i, \Psi] = 0, \tag{3}$$

$$\frac{\partial n_e}{\partial t} + [\phi, n_e] + [u_e, \psi] = 0, \tag{4}$$

$$\frac{\partial}{\partial t}\left(\psi - d_e^2 u_e\right) + [\phi, \psi - d_e^2 u_e] - \rho_s^2 [n_e, \psi] = 0, \tag{5}$$

where $[f, g] = \partial_x f \partial_y g - \partial_y f \partial_x g$ is the canonical Poisson bracket between two generic fields f and g. The four dimensionless parameters appearing in the above equations are the (normalized) electron and ion skin depth, $d_e = (c/\omega_{pe})/L$ and $d_i = (c/\omega_{pi})/L$ respectively, and the (normalized) sonic and ion Larmor radius, $\rho_s = (c_s/\omega_{ci})/L$ and $\rho_i = (v_{ti}/\omega_{ci})/L$ respectively. Here, $c_s = (T_e/m_i)^{1/2}$ is the sound speed based on the electron temperature, $v_{ti} = (T_i/m_i)^{1/2}$ is the ion thermal speed, and the other symbols have their usual meaning. Furthermore, $\Phi = \Gamma_0^{1/2}\phi$ and $\Psi = \Gamma_0^{1/2}\psi$ are the gyro-averaged electrostatic and parallel magnetic potentials, where the symbol $\Gamma_0^{1/2}$ refers to the gyro-averaged operator introduced by Dorland and Hammet [18], that we adopt in its lowest-order Padé approximant form $\Gamma_0^{1/2} = \left(1 - \rho_i^2 \nabla_\perp^2/2\right)^{-1}$. Eqs. (2)-(5) are closed by the parallel component of Ampère's law

$$\nabla_\perp^2 \psi = u_e - \Gamma_0^{1/2} u_i, \tag{6}$$

and by imposing quasi-neutrality on the particle density (not the guiding-center density)

$$n_e = \Gamma_0^{1/2} n_i + \left(\frac{\Gamma_0 - 1}{\rho_i^2}\right)\phi, \tag{7}$$

where the last term of Eq. (7) represents the polarization density due to the variation of the electric field around a gyro-orbit.

The system of equations (2)-(7) describes both the inertial ($\beta_e \ll 2m_e/m_i$) and the kinetic ($\beta_e \gg 2m_e/m_i$) Alfvén wave regimes, whereas for $\beta_e \sim 2m_e/m_i$ the model equations need to be extended to account for the electron Landau damping occuring in this regime $v_{te} \sim v_A$ [19]. Here, the parameter that distinguishes between these regimes is the electron beta, defined as $\beta_e \equiv 2\mu_0 n_0 T_e/B_0^2$, which represents the ratio of the electron thermal pressure to the magnetic pressure.

3. Reconnection rate and field structures of ion guiding centers

In order to investigate the evolution of spontaneous magnetic reconnection instabilities, the system of equations (2)-(7) is solved numerically considering the following static equilibrium:

$$\psi_{eq}(x) = \sum_{n=-11}^{11} a_n e^{inx}, \qquad n_{i_{eq}}(x) = n_{e_{eq}}(x) = n_{eq}, \qquad u_{i_{eq}}(x) = 0, \tag{8}$$

where a_n are the Fourier coefficients of the function $f(x) = 0.1/\cosh^2 x$, and n_{eq} represent a uniform, nondrifting background density. The fields in the model equations are decomposed in a time independent equilibrium and an evolving perturbation that is advanced in time according to a third order Adams-Bashforth algorithm. Double periodic boundary conditions are imposed and a pseudospectral method is used for the space discretization on a domain $\{(x, y) : -\pi \leq x < \pi, -2\pi \leq y < 2\pi\}$, with a resolution up to 2048×256 grid points. The reconnection instability is initiated by perturbing the equilibrium with a small disturbance of the ion guiding-center density defined as $\tilde{n}_i = 10^{-6}(\cos(x + y/2) - \cos(x - y/2))$.

The equilibrium (8) is tearing unstable with linear stability parameter $\Delta' = 59.9$ for the longest wavelength mode in the system $k_y = 2\pi/L_y = 1/2$, with L_y the length of the domain along the y direction. This choice allows us to explore magnetic reconnection in the large-Δ' regime, relevant to the sawtooth oscillations in tokamaks [20], for example, or the Geospace Environmental Modeling (GEM) Challenge [21]. The value of the ion skin depth d_i is taken to be equal to the half width of the magnetic equilibrium scale length L. Considering the challenge to clearly separate all relevant spatial scales of the problem, the electron to ion mass ratio, m_e/m_i, is chosen to be 1/100, making $d_e = (m_e/m_i)^{1/2} d_i = 5 \times 10^{-2}$. This mass ratio is larger than the real one, but it has been shown by Ricci *et al.* [22] that most features of collisionless reconnection with a guide field are not sensitive to the mass ratio, except for the magnitude of the electron velocities in the electron diffusion region. Finally, in order to distinguish ion gyration effects from those of electron pressure gradient and electron inertia, ρ_i and ρ_s are varied independently.

As a first step, we consider a range of parameters such that $\rho_i \ll \rho_s < d_e \ll d_i \lesssim L$. In this regime, with $\rho_s = 2.5 \times 10^{-2}$ and $\rho_i = 10^{-5}$, the instantaneous growth rate of the reconnection instability is shown in Fig. 1(a). The growth rate is defined as $\gamma = d(\ln \delta\psi_X)/dt$, where $\delta\psi_X$ is the reconnected flux at the X-point. After an initial transient ($\gamma_L t \lesssim 1.5$), the reconnection instability evolve through three different stages: the linear phase, scaling as $e^{\gamma_L t}$ (constant growth rate $\gamma_L = 2.9 \times 10^{-3}$) ($1.5 \lesssim \gamma_L t \lesssim 4.5$), followed by the faster-than-exponential phase, during which the growth rate increases up to a peak value $\gamma = 1.3 \times 10^{-2}$ ($4.5 \lesssim \gamma_L t \lesssim 7.7$), and finally the saturation period in which the growth rate slows down ($\gamma_L t \gtrsim 7.7$).

A similar evolution of the reconnection instability is found for $\rho_i \ll d_e < \rho_s \ll d_i \lesssim L$, but with higher linear ($\gamma_L = 4.9 \times 10^{-3}$) and nonlinear growth rates (peak value $\gamma = 1.83 \times 10^{-2}$). Fig. 1(b) shows the instantaneous growth rate for $\rho_s = 0.1$ and $\rho_i = 10^{-5}$. The speed up of the reconnection can be linked to the different dispersive character of the kinetic Alfvén wave respect to the shear Alfvén wave. In fact, the term proportional to ρ_s^2 in Eq. (5) introduces

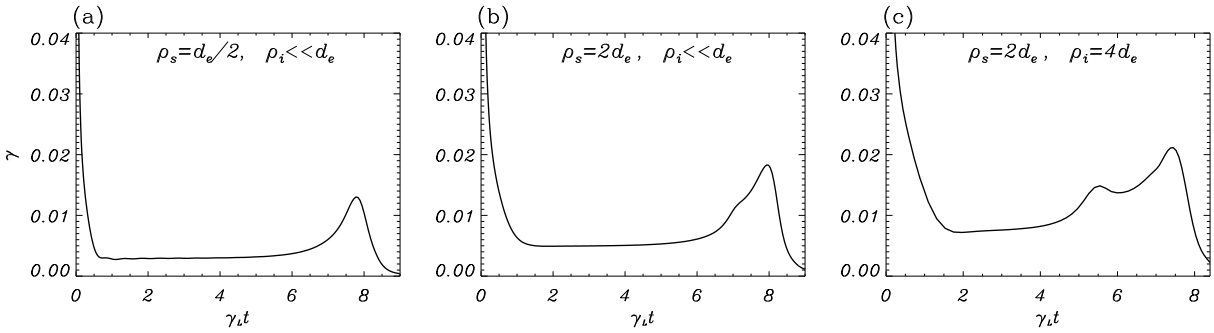

Figure 1. Growth rate of the reconnection instability, $\gamma = d(\ln \delta\psi_X)/dt$, as a function of $\gamma_L t$, for (a) $\rho_s = 2.5\times10^{-2}$, $\rho_i = 10^{-5}$, (b) $\rho_s = 0.1$, $\rho_i = 10^{-5}$, and (c) $\rho_s = 0.1$, $\rho_i = 0.2$. The linear growth rate γ_L is determined numerically: (a) $\gamma_L = 2.9\times10^{-3}$, (b) $\gamma_L = 4.9\times10^{-3}$, and (c) $\gamma_L = 7.3\times10^{-3}$. The values of the electron and ion skin depth are $d_e = 5\times10^{-2}$ and $d_i = 0.5$.

the dynamics of the kinetic Alfvén wave, which has a dispersive character, i.e. $\omega \propto k_\perp^2$, where ω is the wave frequency and $k_\perp$ the wave number. For $\rho_s > d_e$ (equivalent to $\beta_e > 2m_e/m_i$), the structure of the electron inertial region is controlled by the dynamics of the kinetic Alfvén wave rather than the Alfvén dynamics because this region has an intrinsic scale length which is well below the ion inertial length. Indeed, the quadratic dispersion character of the kinetic Alfvén wave leads to an increase in the phase speed ($v_\phi \propto k_\perp$) with decreasing spatial scales and therefore to an increase in the velocity at which the electrons can be ejected from the X-point as the spatial scales of the electron diffusion region decrease [23]. In the absence of a guide field (strictly antiparallel field merging), the counterpart of the electron pressure term is the Hall term in the generalized Ohm's law, which also introduces a high frequency dispersive wave, the whistler, which plays a role analogous to that of the kinetic Alfvén wave [24 - 26].

For plasma parameters of interest to magnetic confinement fusion experiments, ion Larmor radius effects and sonic Larmor radius effects should be considered simultaneously, since $\rho_i/\rho_s = (T_i/T_e)^{1/2} \sim 1$ and $\rho_i/d_e = (\beta_i m_i/2m_e)^{1/2} > 1$, with $\beta_i \equiv 2\mu_0 n_0 T_i/B_0^2$. For this reason and to highlight the contribution of the ion gyration, we consider a regime such that $d_e < \rho_s \lesssim \rho_i \ll d_i \lesssim L$. In particular, the instantaneous growth rate for $\rho_s = 0.1$ and $\rho_i = 0.2$ is shown in Fig. 1(c). In comparison to the cold ion limit, the evolution of the reconnection instability exhibits a novel behaviour: nonlinearly, the growth rate is characterized by two distinct phases of strong increase. After an initial transient, which lasts until $\gamma_L t \lesssim 2$, reconnection evolves through a linear phase from $\gamma_L t \approx 2$ to $\gamma_L t \approx 3$ with $\gamma_L = 7.3\times10^{-3}$, and then develops into a first growth rate acceleration phase that begins at an island width $w \sim d_e$, and persists until $\gamma_L t \approx 5.5$, when $\gamma = 1.49\times10^{-2}$. The first acceleration stage is followed by a phase in which the growth rate decreases until $\gamma_L t \approx 6$, when a second remarkable increase takes place. This second acceleration phase is accompanied by an opening up of the electron parallel velocity layer into an "X"-geometry similar to the island separatrix. Moreover, from $\gamma_L t \gtrsim 7$ also the parallel velocity of the ion guiding centers splits into an "X"-geometry configuration centered at the X-point, but with lower opening compared to the electron velocity. The formation of an "X"-geometry in the current distribution was linked to an increase of the reconnection rate in a number of works [7 - 9, 23 - 28]. Here we observe a similar behaviour in the parallel velocity of the ion guiding centers, which enters the parallel electron momentum equation through Ampère's law. In fact, making use of Eq. (6) we can rewrite Eq. (5) as

$$\frac{\partial}{\partial t}\left(\psi - d_e^2\nabla_\perp^2\psi - d_e^2\Gamma_0^{1/2}u_i\right) + [\phi, \psi - d_e^2\nabla_\perp^2\psi - d_e^2\Gamma_0^{1/2}u_i] - \rho_s^2[n_e, \psi] = 0, \qquad (9)$$

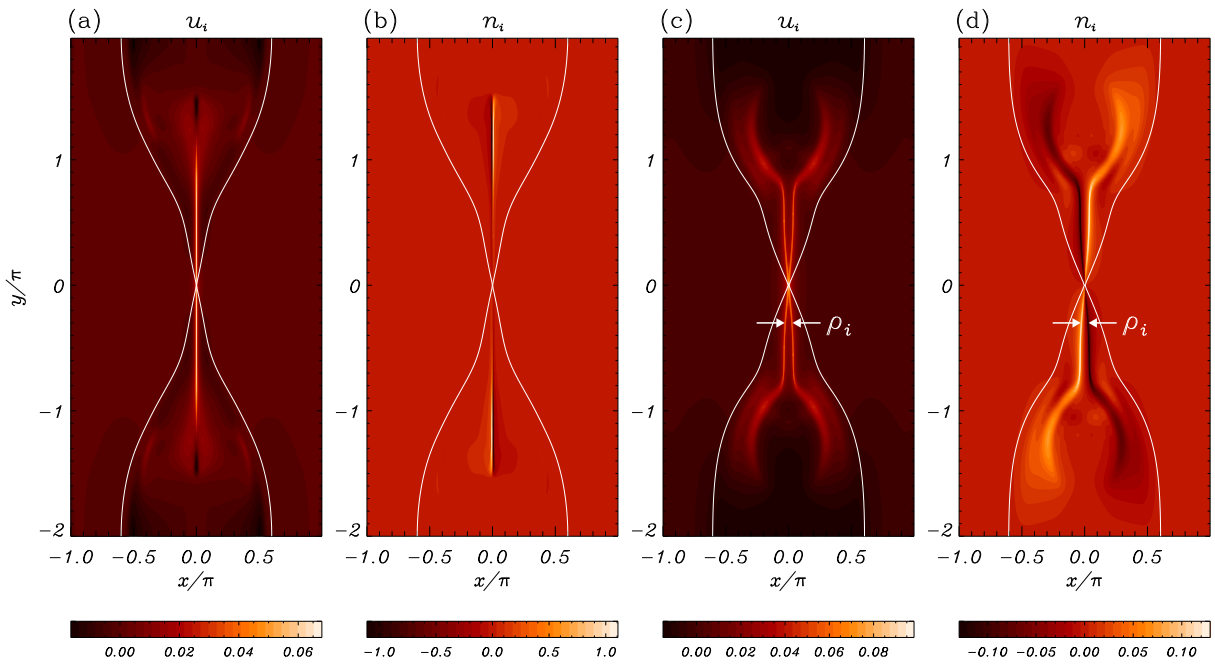

Figure 2. Contour plots of the ion guiding-center parallel velocity u_i and perturbed density n_i at an island width $w \approx 1.2\pi$ for (a)-(b) $\rho_s = 0.1$, $\rho_i = 10^{-5}$, and for (c)-(d) $\rho_s = 0.1$, $\rho_i = 0.2$. The values of the other plasma parameters are: $d_e = 5 \times 10^{-2}$, $d_i = 0.5$. The magnetic island separatrix at the corresponding time have been superimposed (white line). White arrows indicate the length scale ρ_i.

which puts in evidence how the frozen-in condition is violated also due to a term depending on u_i and often neglected in fluid models. However, for low-β regimes the influence of u_i on the rate of reconnection remains small in comparison to the role played by u_e. The increase of the growth rate during the second acceleration phase reaches a peak value $\gamma = 2.12 \times 10^{-2}$ at $\gamma_L t \approx 7.8$. After this time a saturation stage takes place.

The macroscopic structures that develop in the advanced nonlinear phase for the cold ion limit ($\rho_i^2/\rho_s^2 = T_i/T_e \ll 1$) and for the finite ion Larmor radius regime are compared in Fig. 2. Contour plots of u_i and n_i for $\rho_s = 0.1$, $\rho_i = 10^{-5}$ are shown in Figs. 2(a) and 2(b) for an island width $w \approx 1.2\pi$, corresponding at $\gamma_L t \approx 8.3$ in Fig. 1(b). Isocontours of the same fields for $\rho_s = 0.1$, $\rho_i = 0.2$ are shown in Figs. 2(c) and 2(d) for the same island width, corresponding at $\gamma_L t \approx 8$ in Fig. 1(c). In the cold ion limit narrow layer structures aligned with the magnetic equilibrium null line characterize the parallel velocity and perturbed density of the ion guiding centers. Finite values of the ion Larmor radius are identified to be responsible for a splitting of the regions of high ion parallel velocity. The same splitting happens in the regions of high density fluctuations. The result is that the quadrupolar density perturbation of the ion guiding centers, characterized by two regions of enhanced ion density and two regions of depleted ion density (cavities), instead of being aligned along the neutral line, opens on a spatial scale $\sim \rho_i$, as shown in Fig. 2(d). This behaviour is different from what was found for the antisymmetric signature of the quadrupolar electron density perturbation, where the regions of high and low electron density map the separatrices [8, 17, 22, 29 - 31]. The field structures of u_i and n_i were interpreted in terms of the change, due to ion Larmor radius effects, of the advection of two of the four Lagrangian invariants of the model (2)-(7), defined as $I_\pm \equiv \Psi + d_i^2 u_i \pm d_i \rho_i n_i$ [17]. We observe that the splitting of u_i and n_i for large values of ρ_i was not found in Ref. [17],

where a regime of plasma parameters ($d_{e,i}$, $\rho_{s,i}$) four times larger than those of Figs. 1(c), 2(c), 2(d) was investigated (but with the same initial current sheet), in such a way that β_e and β_i remain the same. This is because the excursion of the ions in their Larmor gyration causes a smoothing of u_i and n_i for which ρ_i is the typical scale length [17, 32]. Ion gyration effects also influence the growth rate, that does not exhibit two distinct strong acceleration phases for the plasma parameters $d_e = 0.2$, $d_i = 2$, $\rho_s = 0.2$, $\rho_i = 0.8$, corresponding to the regime $d_e < \rho_s \lesssim \rho_i \sim L \lesssim d_i$.

4. Conclusions

In summary, we have shown that collisionless magnetic reconnection with a guide field undergoes a strong enhancement of the growth rate when a rarefied high temperature plasma is considered. Particularly noteworthy is the fact that the growth rate exhibits two distinct nonlinear acceleration phases when the ion Larmor radius exceeds the electron skin depth and is much less than the magnetic equilibrium shear length. We have also shown that finite values of the ion Larmor radius are responsible to produce an open configuration of the ion guiding-center parallel velocity, that is reminiscent of the cross-shaped configuration that characterize the parallel current density in magnetic reconnection mediated by the kinetic Alfvén wave. The same geometric pattern belongs to the quadrupolar ion guiding-center density perturbation.

Acknowledgments

The authors would like to acknowledge fruitful conversations with Dario Borgogno, Emanuele Tassi, Ahmet Aydemir and Vladimir Lakhin. One of us (L.C.) is grateful for the hospitality of the Institute for Fusion Studies at the University of Texas at Austin, where part of this work was done. This work was supported by the European Community under the contracts of Association between EURATOM and ENEA and by the U.S. Department of Energy under Contract No. DE-FG02-04ER-54742. The views and opinions expressed herein do not necessarily reflect those of the European Commission.

References

[1] Priest E R and Forbes T G 2000 *Magnetic Reconnection: MHD Theory and Applications* (Cambridge: Cambridge University Press)
[2] Biskamp D 2000 *Magnetic Reconnection in Plasmas* (Cambridge: Cambridge University Press)
[3] Hastie R J 1998 *Astrophys. Space Sci.* **256**, 177
[4] Bhattacharjee A 2004 *Annu. Rev. Astron. Astrophys.* **42**, 365
[5] Yamada M, Kulsrud R and Ji H 2010 *Rev. Mod. Phys.* **82**, 603
[6] Birn J and Priest E R (ed) 2007 *Reconnection of Magnetic Fields: Magnetohydrodynamics and Collisionless Theory and Observations* (Cambridge: Cambridge University Press)
[7] Aydemir A Y 1992 *Phys. Fluids B* **4**, 3469
[8] Kleva R G, Drake J F and Waelbroeck F L 1995 *Phys. Plasmas* **2**, 23
[9] Rogers B and Zakharov L 1996 *Phys. Plasmas* **3**, 2411
[10] Cafaro E, Grasso D, Pegoraro F, Porcelli F and Saluzzi A 1998 *Phys. Rev. Lett.* **80**, 4430
[11] Grasso D, Califano F, Pegoraro F and Porcelli F 2000 *Plasma Phys. Rep.* **26**, 512
[12] Porcelli F, Borgogno D, Califano F, Grasso D, Ottaviani M and Pegoraro F 2002 *Plasma Phys. Control. Fusion* **44**, 389
[13] Bhattacharjee A, Germaschewski K and Ng C S 2005 *Phys. Plasmas* **12**, 042305
[14] Biancalani A and Scott B D 2012 *Europhys. Lett.* **97**, 15005
[15] Waelbroeck F L and Tassi E 2012 *Commun. Nonlinear Sci. Numer. Simulat.* **17**, 2171
[16] Snyder P B and Hammett G W 2001 *Phys. Plasmas* **8**, 3199
[17] Comisso L, Grasso D, Tassi E and Waelbroeck F L 2012 *Phys. Plasmas* **19**, 042103
[18] Dorland W and Hammett G W 1993 *Phys. Fluids B* **5**, 812
[19] Hammett G W, Dorland W and Perkins F W 1992 *Phys. Fluids B* **4**, 2052
[20] Angioni C, Pochelon A, Gorelenkov N N, McClements K G, Sauter O, Budny R V, de Vries P C, Howell D F, Mantsinen M, Nave M F F, Sharapov S E and contributors to the EFDA-JET Workprogramme 2002 *Plasma Phys. Control. Fusion* **44**, 205

[21] Birn J, Drake J F, Shay M A, Rogers B N, Denton R E, Hesse M, Kuznetsova M, Ma Z W, Bhattacharjee A, Otto A and Pritchett P L 2001 *J. Geophys. Res.* **106**, 3715
[22] Ricci P, Brackbill J U, Daughton W and Lapenta G 2004 *Phys. Plasmas* **11**, 4102
[23] Rogers B N, Denton R E, Drake J F and Shay M A 2001 *Phys. Rev. Lett.* **87**, 195004
[24] Biskamp D, Schwarz E and Drake J F 1997 *Phys. Plasmas* **4**, 1002
[25] Shay M A and Drake J F 1998 *Geophys. Res. Lett.* **25**, 3759
[26] Drake J F, Shay M A and Swisdak M 2008 *Phys. Plasmas* **15**, 042306
[27] Lazzaro E, Ferrero M, Gianoli L and Valdettaro L 2000 *Phys. Scr.* **61**, 624
[28] Cassak P A, Shay M A and Drake J F 2005 *Phys. Rev. Lett.* **95**, 235002
[29] Pritchett P L 2005 *Phys. Plasmas* **12**, 062301
[30] Drake J F, Shay M A, Thongthai W and Swisdak M 2005 *Phys. Rev. Lett.* **94**, 095001
[31] Grasso D, Tassi E and Waelbroeck F L 2010 *Phys. Plasmas* **17**, 082312
[32] Del Sarto D, Marchetto C, Pegoraro F and Califano F 2011 *Plasma Phys. Control. Fusion* **53**, 035008